Relating resting-state fMRI and EEG brain connectivity across frequency bands

Fani Deligianni[1], Maria Centeno[1], David W. Carmichael[1], and Jonathan D. Clayden[1]
[1]*Institute of Child Health, UCL, London, United Kingdom*

Audience: To those interested in the relationship between resting-state EEG and fMRI connectivity.

Purpose: It has been shown that the resting-state (rs) networks observed with fMRI reflect electrophysiological activity [1-3]. However, questions remain regarding which EEG features most closely reflect rs-fMRI networks. For example, significant spatial agreement with fMRI derived networks emerged from MEG data filtered in the β and α frequency bands [1, 2]. Whereas, work in anesthetised animals with intracranial EEG suggested that the rs-fMRI signal correlated with the EEG power coherence in low-frequency bands [3]. We relate the covariance structure of the Hilbert envelope of the source localised electrophysiological signal to the covariance matrices derived from rs-fMRI. This allows direct comparison of EEG and fMRI connectivity. Statistical inference has been shown to be a useful tool in examining the relationship between brain connectivity variables [4, 5]. We use statistical inference based on sparse Canonical Correlation Analysis (sCCA) [6] to predict EEG brain connectivity from fMRI connectivity and vice-versa and we identify the most prominent connections that contribute to this relationship.

Methods: Simultaneous EEG-fMRI was acquired from 17 adult volunteers. Scalp EEG was recorded using a 64-channel MR-compatible electrode cap (BrainCap MR). A T2*-weighted gradient-echo EPI sequence with 300 volumes was acquired at 1.5T: TR/TE=2160/30 msec, 30 slices with thickness 3.0 mm (1mm gap), effective voxel size 4.0×3.3×3.3 mm, flip angle 75^0, FOV 210×210×120 mm. A T1-weighted structural image was also obtained.

EEG was corrected for scanner and cardiac pulse related artefacts using Brain Vision Analyzer 2. It was down-sampled to 250 Hz and frequency filtered into five bands: δ(1-4Hz), θ(4-8Hz), α(8-13Hz), β(13-30Hz) and γ(30-70Hz). Frequency filtered EEG data were projected into source space using beamforming as implemented in SPM12b [2, 7]. The signal was segmented into (fMRI) TR epochs. The average envelope of the signal was estimated for each segment based on the absolute value of the Hilbert transform. Preprocessing of the fMRI data involves removing the first five volumes, motion correction, low pass filtering and spatial smoothing with FSL. Both pre-processed fMRI and the averaged envelope of the EEG signals were averaged within cortical gray matter regions derived from Freesurfer's anatomical parcellation of the T1-weighted image. For this reason, the Freesurfer parcellation was propagated to native fMRI and MNI space, respectively, with non-rigid registration. For each cortical region, the fMRI signal is averaged across all voxels, whereas the EEG signal is projected from sensor space to points randomly drawn from the region. The region's centre of mass is always included whereas the number of points is proportional to region's volume.

Connectivity matrices were derived based on the precision matrix, the inverse of covariance of the averaged time series signal. This reflects partial correlation and it has been estimated based on a shrinkage approach [8]. We use sCCA to learn sparse vectors u, v that maximize the linear relationship between EEG (**X**) and rs-fMRI (**Y**) connectivity data as in eq.1 [6]. Sparsity is achieved based on lasso penalties c_1, c_2 that result in simultaneous multivariate dimensionality reduction and selection of the most relevant connections. Subsequently, rs-fMRI connectivity $\hat{\mathbf{Y}}$ is predicted from an unseen EEG connectivity matrix $\tilde{\mathbf{X}}$ according to eq.2. *Vice-versa* EEG ($\hat{\mathbf{X}}$) connectivity can be predicted from rs-fMRI connectivity ($\tilde{\mathbf{Y}}$), eq.3. **D** is a diagonal matrix with the canonical correlation scores. We estimated the similarity between connectivity matrices based on a distance metric that quantifies differences in the space of covariance matrices as in eq.4 [4, 5, 9].

$$\max_{u,v} u^T \mathbf{X}^T \mathbf{Y} v \;,\; \|u\|_1 \le c_1,\ \|v\|_1 \le c_2 \quad \textbf{[eq.1]} \qquad \hat{\mathbf{Y}} = \left(u\tilde{\mathbf{X}}\right)^{-1} \mathbf{D} v^{-1} \quad \textbf{[eq.2]} \qquad \hat{\mathbf{X}} = \left(\left(\tilde{\mathbf{Y}} v\right)^T\right)^{-1} \mathbf{D} u^{-1} \quad \textbf{[eq.3]}$$

$$d_{AI}\left(\mathbf{A},\mathbf{B}\right) = \left\| \mathrm{tr}\left(\log\left(\mathbf{A}^{-1/2}\mathbf{B}\mathbf{A}^{-1/2}\right)\right)\right\| \quad \textbf{[eq.4]}$$

Results: Fig. 1 summarises the results from three experiments. Firstly, it shows the comparison of the original EEG and rs-fMRI precision matrices across bands before sCCA training. These results demonstrate that the distance between EEG and rs-fMRI connectivity matrices is minimised in the β band, and the α and γ bands follow it closely. The highest distance was observed for the δ and θ bands. Fig. 1 also depicts leave-one-out cross validation results of the prediction performance of rs-fMRI based on EEG and the prediction performance of EEG from rs-fMRI across bands. c_1, c_2 have been optimised in each cross-validation loop according to a permutation-based algorithm [6]. The number of components is estimated as the min of the ranks of the variables **X**, **Y**. The ability to predict a rs-fMRI precision matrix from an EEG precision matrix remains relatively similar across bands and it is better than the prediction of an EEG precision matrix from a rs-fMRI connectivity matrix. Furthermore, the prediction performance of EEG from fMRI is modulated considerably by the EEG frequency band and follows similar pattern to the distance of the original precision matrices. As expected training improves the similarity of the predicted matrices to the measured connectivity matrices in almost all cases. Fig. 2(â) shows the average rs-fMRI brain network. Brain regions are represented with spheres. Their centers and radius represent the center of masses of each underlying region and its relative size, respectively. The color-coding corresponds to different brain lobes. Fig. 2(a-e) shows the average EEG brain network for bands δ, θ, α, β and γ, respectively. It is apparent that the most prominent rs-fMRI connections are inter-hemispheric. Fig. 2 second and third lines show bootstrap results of 1000 iterations with replacement with repetition that identify the most prominent connections from rs-fMRI (v) and EEG (u) brain connections, respectively, which contribute in maximising the linear relationship between **Y** and **X** in eq.1. In order to alleviate the influence of c_1, c_2 on the results, we estimate them in each bootstrap iteration. Fig. 2 bottom two lines show the connections that are present in rs-fMRI and EEG frequency bands for over 59% and 55% of bootstrap iterations, respectively.

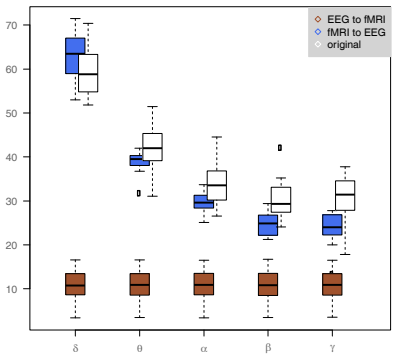

Fig. 1: Distance of EEG from rs-fMRI brain connectivity based on d_{AI}, eq. 4.

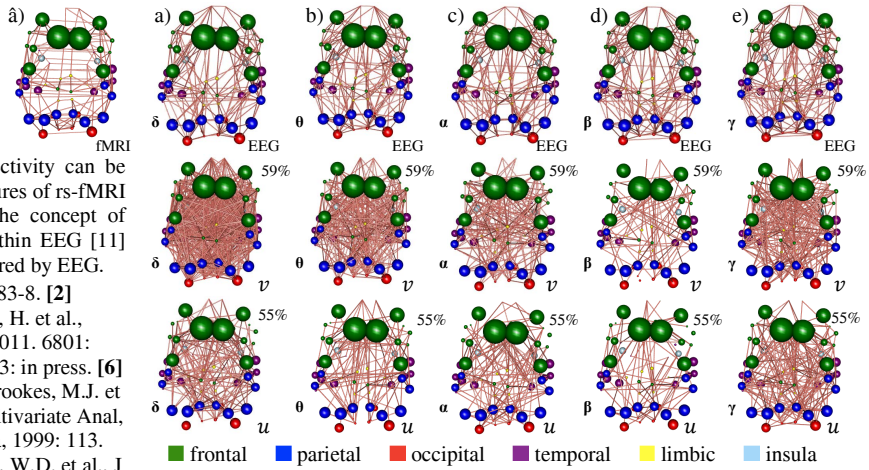

Fig. 2: Average brain networks and bootstrap results of the sCCA algorithm.

Conclusions: We compare the precision matrices derived from EEG and rs-fMRI signal both directly and with the means of statistical prediction. We provide quantitative evidence that support the hypothesis that the β band EEG activity best reflects spontaneous cognitive operations during conscious rest [10]. We have demonstrated that fMRI connectivity can be predicted from EEG in any band indicating that there are signatures of rs-fMRI dynamics across EEG frequencies. This is consistent with the concept of nested oscillations and cross spectral coupling often found within EEG [11] and it may reflect the greater dynamic information content captured by EEG.

References: **[1]** Brookes, M.J. et al., PNAS, 2011. 108(40): 16783-8. **[2]** Brookes, M.J. et al., Neuroimage, 2011. 56(3): 1082-104. **[3]** Lu, H. et al., PNAS, 2007. 104(46): 18265-9. **[4]** Deligianni, F. et al., IPMI, 2011. 6801: 296-307. **[5]** Deligianni, F. et al., IEEE Trans Med Imaging, 2013: in press. **[6]** Witten, D.M. et al., Stat Appl Genet Mol Biol, 2009. 8(1). **[7]** Brookes, M.J. et al., Neuroimage, 2012. 63(2): 910-20. **[8]** Ledoit, O. et al., J Multivariate Anal, 2004. 88(2): 365-411. **[9]** Forstner, W. et al., Qua vadis geodesia, 1999: 113. **[10]** Laufs, H. et al., PNAS, 2003. 100(19): 11053-8. **[11]** Penny, W.D. et al., J Neurosci Methods, 2008. 174(1): 50-61.